Proceedings of the
Annual Stability Conference
Structural Stability Research Council
Atlanta, Georgia, April 21-24, 2026

Cross-section design of stainless steel H.S.S.

Nathalie Fawaz[1], Nicolas Boissonnade[2]

Abstract

Stainless steel is increasingly used in structural and architectural applications due to its corrosion resistance, durability and fire performance. Its continuous, non-linear stress-strain response and pronounced strain hardening, however, render carbon-steel design rules inappropriate. Although standards such as Eurocode 3 and A.I.S.C. contain stainless steel provisions, they often lack accuracy and consistency, hence the need for stainless steel specific design recommendations.

This study examines the cross-sectional resistance of welded stainless steel rectangular and square hollow sections under axial compression or uniaxial bending about both principal axes. Advanced non-linear finite element models were developed, validated against 26 tests and used in a parametric study of over 2 160 simulations covering various geometries, loading and material responses. Based on these data, a design framework employing the Overall Interaction Concept (O.I.C.) is proposed. Comparative and reliability analyses show that the O.I.C. provides improved accuracy, consistency and safety compliance, offering an efficient design method for stainless steel tubular sections.

1. Introduction

Stainless steels offer durability, corrosion resistance and favorable fire performance, enabling slender, long-lasting structures (Gardner, 2008). Over the past few decades, extensive research has been undertaken to develop structural design principles that account for these beneficial characteristics. These efforts have led to the establishment of international design standards such as EN 1993-1-4 or A.I.S.C. Stainless steel characteristic rounded stress-strain material response lacks a well-defined yield point and a distinct yield plateau, and exhibits significant strain hardening (see typical curves for ferritic, austenitic and duplex grades shown in Fig. 1); these characteristics fundamentally differ from carbon steel, and consequently invalidate carbon steel-based design provisions.

[1] PhD student, St Joseph University, <nathalie.fawaz@net.usj.edu.lb>
[2] Professor, Laval University, <nicolas.boissonnade@gci.ulaval.ca>

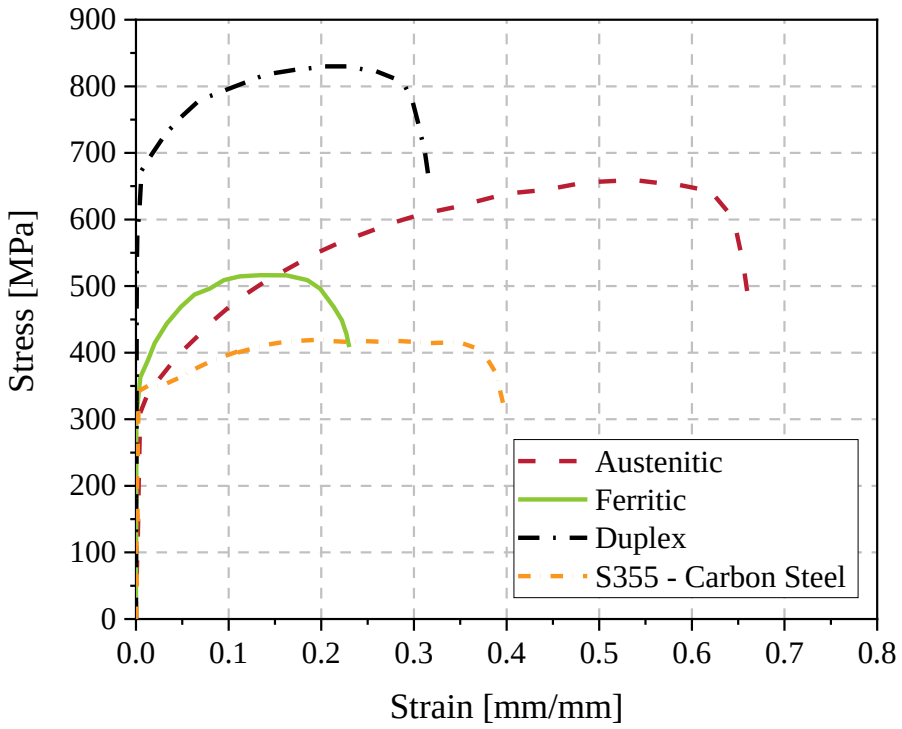

Figure 1. Comparison between stainless steel and regular carbon-steel.

Tubular stainless steel sections exhibit high bending and compression resistance, widely studied by Huang et al. (Huang, 2012), Ashraf et al. (Ashraf, 2006), Young et al. (Young, 2005) or Gardner (Gardner, 2019), among others. The Continuous Strength Method (C.S.M., Gardner et al. (Gardner, 2023)) is currently the leading European approach for very compact stainless steel sections, exploiting strain hardening reserves. As a result of these research efforts, major design codes, (Eurocode 3, 2015) and (A.I.S.C., 2013), have been revised and expanded to incorporate dedicated provisions for stainless steel cross-sections and members.

The Overall Interaction Concept (O.I.C., Boissonnade at al (Boissonnade, 2017)) is a modern design method developed to address the need for more accurate and efficient structural design methods; it relies on the resistance-instability interaction, eliminates cross-section classification and avoids discontinuities as well as long, complex design calculations inherent in the Effective Width Method (E.W.M.). Initially developed for carbon steel and later extended to fire design (Paquet, 2021) and stainless steel I-sections (Gagné et al. (Gagné, 2020)), the O.I.C. accounts for plate-element interaction and typically yields more economical designs (Nseir, 2015) (Hayeck, 2016).

The present study extends the O.I.C. to stainless steel hollow sections, characterized by possibly important strain hardening reserves and the absence of a well-defined plastic plateau. Section 2 describes the key parameters considered in the numerical framework (non-linear shell FE models) and its validation process. Owing to a strong correlation with test results, the validated models are extensively used to generate reference data for assessing the proposed O.I.C. based design approach, detailed in Section 3. Section 4 evaluates accuracy, whereas Section 5 summarizes safety analyses.

2 Numerical modelling: generation, validation, and parametric studies

2.1 General

FE analyses were performed in ABAQUS (Abaqus, 2011) using four-node S4R shell elements. These elements effectively capture cross-sectional response in Geometrically and Materially Non-linear Analyses with Imperfections (G.M.N.I.A.), Linear Buckling Analyses (L.B.A.) and Materially Non-linear Analyses (M.N.A.). G.M.N.I.A. used the Riks method, and L.B.A. relied primarily on subspace iteration. For all simulations, the member length was fixed at three times the average of section height and width to avoid global instability while minimizing boundary effects.

Material laws were defined using the two-stage Ramberg-Osgood (R-O) model (Gardner et al. (Gardner, 2006)) (Ramberg et al. (Ramberg, 1943)) (Hill, 1944) (Mirambell et al. (Mirambell, 2000)) (Rasmussen, 2003). Engineering stress-strain curves were converted to true stress and logarithmic plastic strain using:

$$\sigma_{true} = \sigma_{nom} \cdot \left(1 + \varepsilon_{nom}\right) \tag{1}$$

$$\varepsilon_{\ln}^{pl} = \ln\left(1 + \varepsilon_{nom}\right) - \frac{\sigma_{true}}{E} \tag{2}$$

where E is the Young's modulus, σ_{true} is the true stress, ε_{ln}^{pl} is the logarithmic plastic strain, and

σ_{nom} and ε_{nom} are the engineering stress and engineering strain, respectively.

2.2 Material response

Three representative grades – 1.4301 (austenitic), 1.4003 (ferritic) and 1.4362 (duplex) – were thought to be the most prevalent and therefore selected. Each was modeled using the two-stage R-O formulation (Eq. (3) (Gardner et al. (Gardner, 2004)). Stress-strain curves were represented by eight linear segments, refined in highly curved regions, ensuring close agreement with the analytical model (Fig. 2). Material parameters are summarized in Table 1.

$$\begin{cases} \varepsilon = \dfrac{\sigma}{E_0} + 0.002 \cdot \left(\dfrac{\sigma}{\sigma_{0.2}}\right)^{n} & \text{for } \sigma \le \sigma_{0.2} \\ \varepsilon = \dfrac{\left(\sigma - \sigma_{0.2}\right)}{E_{0.2}} + \left(0.008 - \dfrac{\sigma_{1.0} - \sigma_{0.2}}{E_{0.2}}\right) \cdot \left(\dfrac{\sigma - \sigma_{0.2}}{\sigma_{1.0} - \sigma_{0.2}}\right)^{n'_{0.2,1.0}} + \varepsilon_{t\,0.2} & \text{for } \sigma \ge \sigma_{0.2} \end{cases} \tag{3}$$

Where $E_{0.2} = \frac{\sigma_{0.2}\, x\, E_0}{\sigma_{0.2} + 0.002\, x\, lnE_0}$ and $n'_{0.2,1.0}$are strain hardening coefficients that defines a curve

passing through $\sigma_{0.2}$ and $\sigma_{1.0}$.

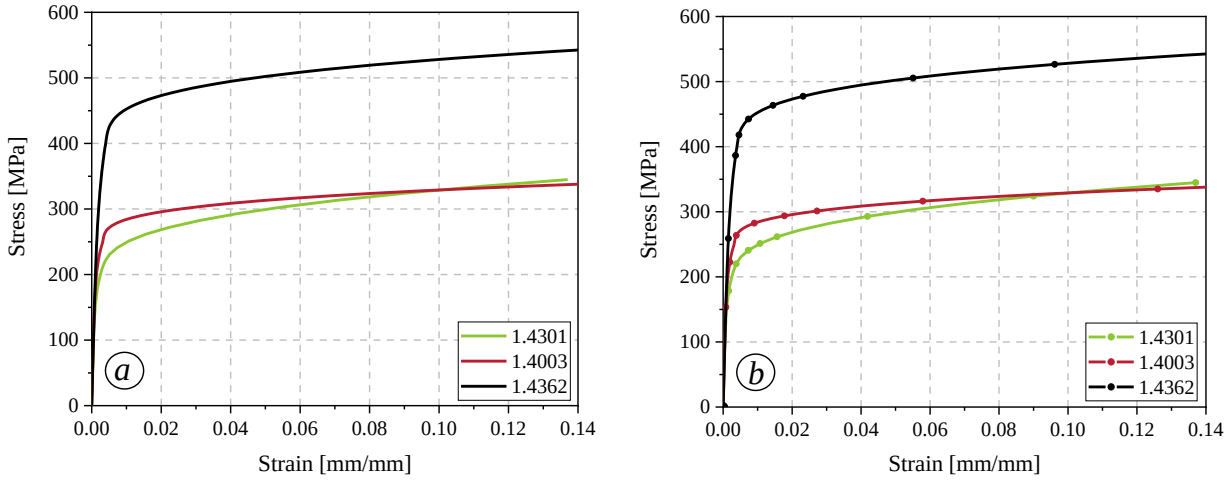

Figure 2. a) Original σ–ε relationship (two-stage R-O) and b) Eight-segments approximations for F.E. simulations.

Table 1: Material parameters data.

Material grades	**1.4301**	**1.4003**	**1.4362**
E_0 [N/mm^2]	200 000	210 000	200 000
$E_{0.2}$ [N/mm^2]	16 092	16 458	33 333
$\sigma_{0.2}$ [N/mm^2]	210	250	400
σ_u [N/mm^2]	520	450	630
$\sigma_{1.0}$ [N/mm^2]	252	286	458
n [–]	6	7	5
$n'_{0.2,1.0}$ [–]	2.7	3.3	3.35

2.3 Mesh sensitivity study

A mesh-refinement study evaluated accuracy versus computational cost using mesh Types 1-5 (Fig. 3). Types 3 and 4 matched the accuracy of Type 5 (reference), while Type 3 provided optimal efficiency. It was adopted for all simulations (Figs. 3-4).

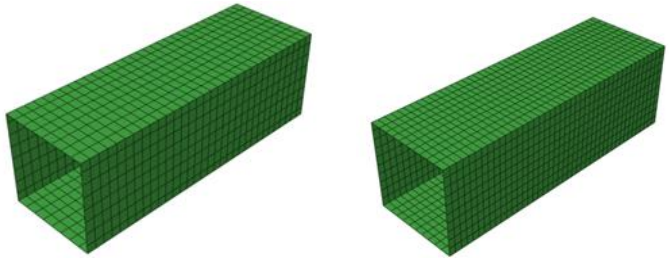

Type 1 Type 2

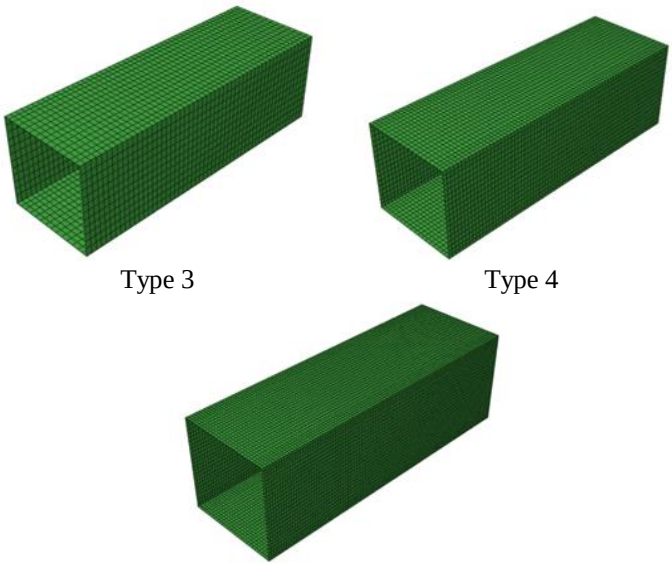

Figure 3. Mesh configurations for square hollow sections.

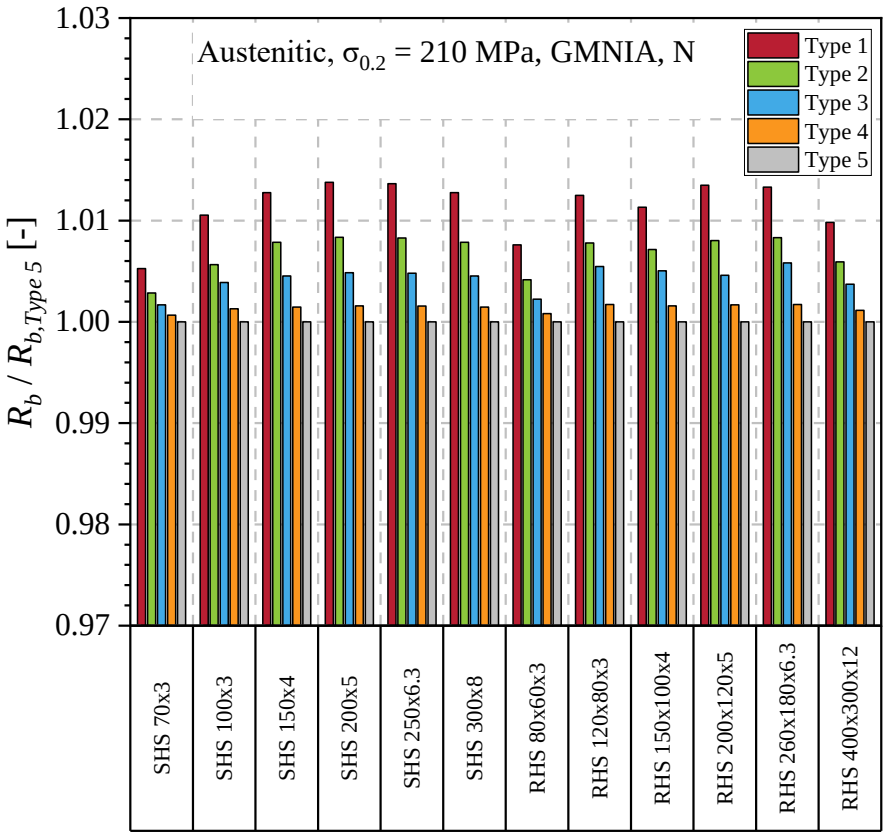

Figure 4. Mesh sensitivity study, G.M.N.I.A. results for RHS and SHS sections in compression ($\sigma_{0.2}$ = 210 MPa).

2.4 Loading and support conditions

Classical fork supports were used at both ends (Fig. 5). Plate nodes were linked to three master nodes enforcing axial displacement and rotations, while warping was neglected due to high torsional rigidity within the tube sections. Consequently, the axial displacement of any other node in the end section – the "*x*-constrained" nodes in Fig. 5 – is fully determined by the movements of three independent master nodes alone (the "*x*-free" nodes shown in blue). Accordingly, suitable constraint equations ensured consistency with Bernoulli kinematics. Additional lateral restraints prevented end-region local buckling. Loads (N, M_y, M_z) were applied through four end nodes to preserve symmetry (see Fig. 6). Previous load-path sensitivity studies (Nseir, 2015) (Hayeck, 2016) confirmed this modeling strategy.

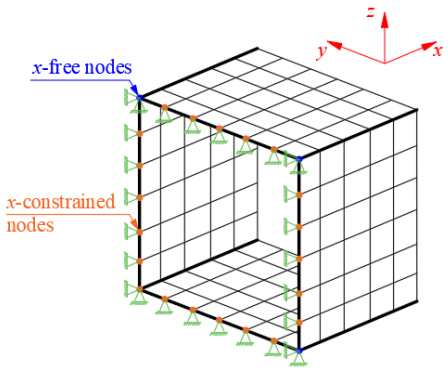

Figure 5. End-section modelling: transverse supports and boundary conditions (Dahboul et al. (Dahboul, 2025)).

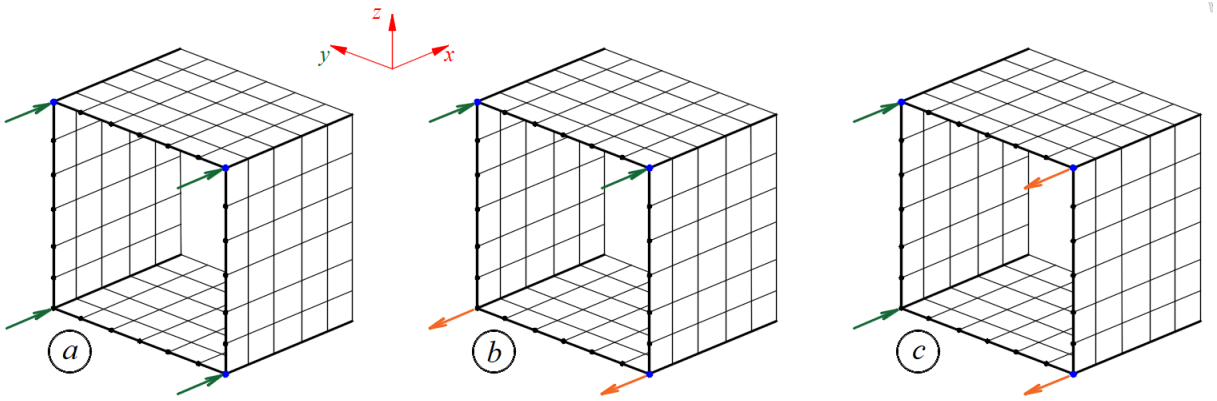

Figure 6. Application of load through nodal forces – a) Compression N – b) Major-axis bending M_y – c) Minor-axis bending M_z (Dahboul et al. (Dahboul, 2025)).

2.5 Material and geometrical initial imperfections

Residual stresses in welded stainless steel sections differ from those in carbon steel sections and arise from sheet forming, welding and differential cooling (Gardner et al. (Gardner, 2006)) (Huang et al. (Huang, 2012)) (Quach et al. (Quach, 2009a)) (Quach et al. (Quach, 2009b)) (Withers et al. (Withers, 2001)). In each plate of the welded hollow section, two tensile peaks (σ_{sft} or σ_{swt}) and one compressive peak (σ_{sfc} or σ_{swc}) were included. Tensile peaks were set to 0.8 $\sigma_{0.2}$ (austenitic) and 0.6 $\sigma_{0.2}$ (duplex/ferritic). Compressive peaks were computed from equilibrium (Eqs. (4-5)), using parameters defined in Figs. 7a-7b and Table 2.

Following recommendations from Nseir et al. (Nseir, 2016), local geometric imperfections consisted of a sinusoidal shape with three half-waves (Fig. 8), introduced without altering corner geometry. Buckling lengths a_w and a_f were defined according to fabrication method (more precisely, $a_w = h - t - 2 \cdot r$ and $a_f = b - t - 2 \cdot r$ for hot-rolled sections, and $a_w = h - t$ and $a_f = b - t$ for welded shapes, and imperfection amplitudes $a_w / 200$ and $a_f / 200$ were used; the half-period equalled 0.5 ($a_w + a_f$).

$$\sigma_{sfc} = \frac{2 \cdot e + f}{b_f - (2 \cdot e + f)} \cdot \sigma_{sft} \tag{4}$$

$$\sigma_{swc} = \frac{2 \cdot g + h}{h_w - (2 \cdot g + h)} \cdot \sigma_{wft} \tag{5}$$

The symbols are defined in Fig. 7 and Table 2.

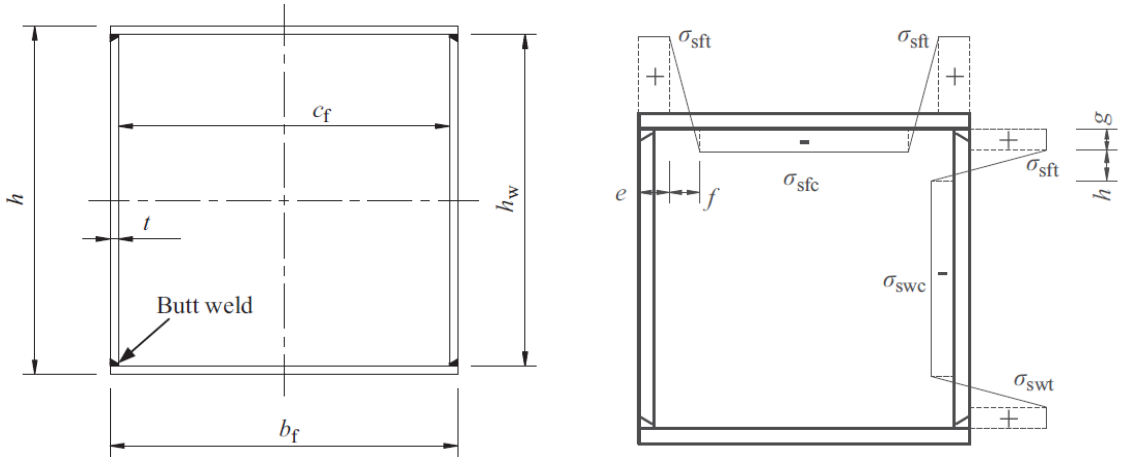

Figure 7. a) Identification of symbols and weld locations for the specimens (Yuan et al. (Yuan, 2014)) – b) Typical residual stresses distributions from ECCS (ECCS, 1984) (ECCS, 1976) and BSK 99 (BSK 99, 2003) models for carbon steel, adopted as the basis for the predictive models of stainless steel.

Table 2: Residual stress distribution parameters in the predictive model for welded stainless steel box sections.

Alloy	**Ratio**	$\sigma_{sft} = \sigma_{swt}$	***e***	***f***	***g***	***h***
Austenitic	$h / t \, (b_f / t) < 20$	$0.8 \, \sigma_{0.2}$	0	$5 \, t_f$	0	$5 \, t_w$
	$h / t \, (b_f / t) \geq 20$	$0.8 \, \sigma_{0.2}$	$t_w + 0.025 \, c_f$	$5 \, t_f$	$0.025 \, h_w$	$5 \, t_w$
Duplex, ferritic	$h / t \, (b_f / t) < 20$	$0.6 \, \sigma_{0.2}$	0	$5 \, t_f$	0	$5 \, t_w$
	$h / t \, (b_f / t) \geq 20$	$0.6 \, \sigma_{0.2}$	$t_w + 0.025 \, c_f$	$5 \, t_f$	$0.025 \, h_w$	$5 \, t_w$

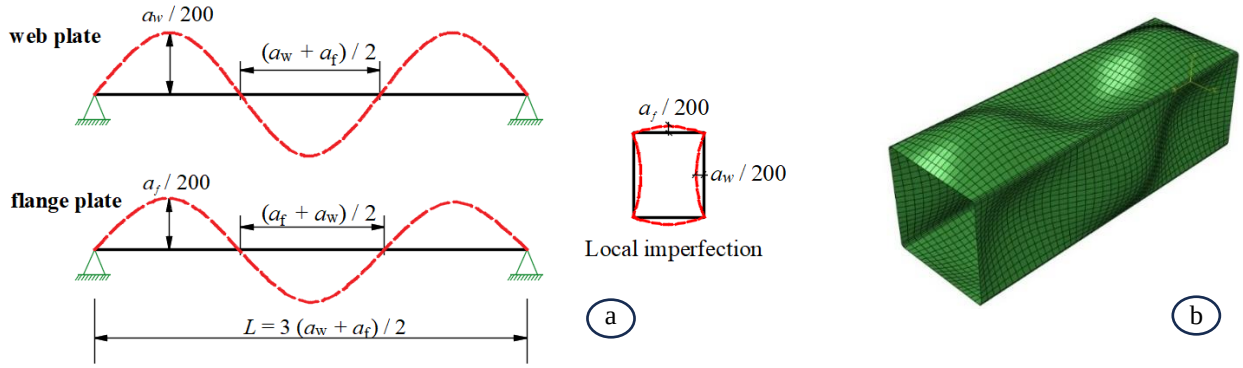

Figure 8. Local imperfections – a) Definition of amplitude and wavelength – b) Overview of the F.E. mesh's original imperfect geometry (magnified).

2.6 Validation of numerical models using experimental data

Because of limited data for welded stainless steel sections, validation was based on carbon steel cold-formed sections, whose corner strength enhancements were modeled following Karren (Karren, 1967), Van den Berg et al. (Van den Berg, 1992), Ashraf et al. (Ashraf, 2005), Cruise et al. (Cruise, 2008), and Gardner et al. (Gardner, 2004). Eqs. (6)-(8) define enhanced proof and ultimate stresses in corner regions (Fig. 9). Membrane residual stresses were omitted, consistent with prior findings (Gardner et al. (Gardner, 2004)) (Ellobody et al. (Ellobody, 2005)).

A database of 26 tests – 15 from Gardner et al. (Gardner, 2004), 7 from Zhao et al. (Zhao, 2015) (Zhao, 2016) and 4 from Afshan (Afshan, 2014) – was assembled. All geometric, material, imperfection, and boundary conditions were carefully reproduced in the FE models. Fig. 10 compares numerical and experimental responses, and Table 3 summarizes peak loads. Strong agreement was observed between the experimental and numerical results. Excluding four outlier tests (S1, S18, S21, S24), the FE-to-test ratio shows a mean deviation of 3% and CoV of 6%, confirming high predictive accuracy. Fig. 11 further demonstrates close agreement in load–displacement behavior and failure modes. Altogether, this confirms that the F.E. models are accurate, reliable and suitable for conducting parametric studies on welded stainless steel sections, as detailed in the following section.

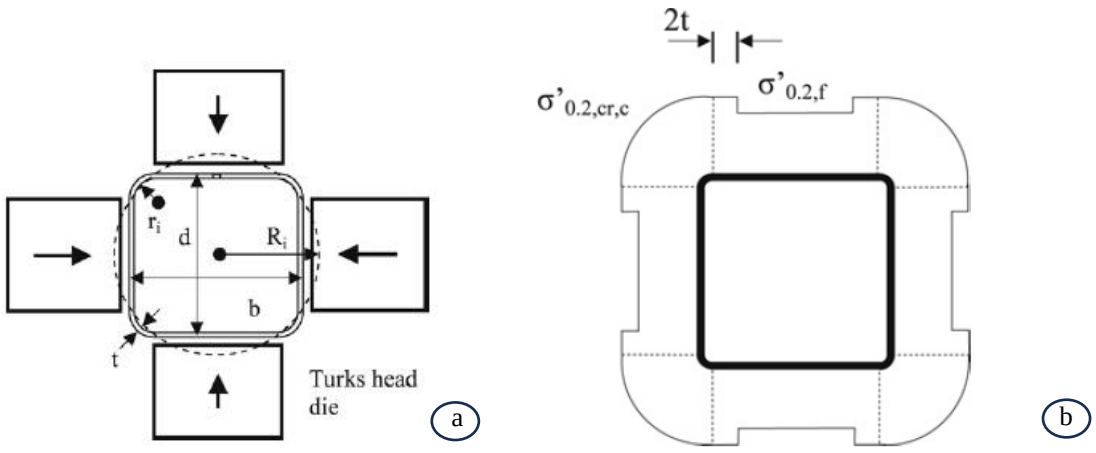

Figure 9. a) Cold rolling of a box section – b) Proposed distributions of 0.2% proof stress for cold-rolled box sections (Cruise et al. (Cruise, 2008)).

$$\sigma'_{0.2,f} = \frac{0.85 \cdot \sigma_{0.2,mill}}{-0.19 + \frac{1}{12.42 \cdot \left(\frac{\pi \cdot t}{2 \cdot (b+d)} \right) + 0.83}} \quad (6)$$

$$\sigma'_{ult,f} = \sigma_{0.2,mill} \cdot \left(0.19 \cdot \left(\frac{\sigma'_{0.2,f}}{\sigma_{0.2,mill}} \right) + 0.85 \right) \quad (7)$$

$$\sigma'_{0.2,cr,c} = 0.83 \cdot \sigma'_{ult,f} \quad (8)$$

Table 3: Documented geometric parameters of specimens and F.E. vs test results.

Reference	Name of specimen	*h* [*mm*]	*b* [*mm*]	*t* [*mm*]	*r* [*mm*]	*L* [*mm*]	Meas. imp. [*mm*]	FE ult. load [*kN*]	Exp. ult. load [*kN*]	F_{FE} / $F_{Exp.}$ [–]
Gardner et al. (Gardner, 2004)	S1	79.80	79.90	3.68	4.60	400.20	0.043	588	727	0.81
	S2	100.20	100.00	1.91	1.30	400.50	0.021	194	197	0.99
	S3	150.40	149.90	3.79	5.80	449.90	0.072	718	726	0.99
	S4	149.90	99.90	3.82	5.60	450.40	0.055	625	660	0.95
	S5	100.00	50.10	5.96	5.50	300.10	0.021	1339	1217	1.10
Zhao et al. (Zhao, 2015)	S6	100.00	99.90	4.65	2.10	349.90	0.015	978	1057	0.93
	S7	120.30	120.10	4.65	5.80	399.90	0.039	931	928	1.00
	S8	150.60	100.00	5.87	7.10	450.10	0.043	1300	1324	0.98
	S9	150.10	100.20	7.75	9.70	450.00	0.028	1915	1825	1.05
	S10	150.40	150.00	8.04	11.20	449.80	0.015	3266	3258	1.00
Gardner et al. (Gardner, 2004)	S11	120.10	80.20	2.93	4.60	359.90	0.038	442	452	0.98
	S12	120.00	80.30	5.85	7.00	360.10	0.016	1371	1465	0.94
	S13	100.10	100.10	2.84	1.50	399.80	0.022	442	496	0.89
	S14	99.80	99.90	3.84	4.50	399.80	0.038	767	779	0.98
	S15	100.10	100.10	5.94	5.80	399.80	0.027	1507	1513	1.00
	S16	100.10	100.70	7.97	8.00	400.00	0.031	1651	1797	0.92
	S17	60.00	40.00	3.82	2.90	179.60	0.017	518	497	1.04
	S18	99.80	49.80	1.85	2.30	300.60	0.139	151	182	0.83
	S19	100.10	50.00	2.89	3.10	300.00	0.055	399	415	0.96
	S20	99.80	49.80	3.68	3.60	300.60	0.032	564	627	0.90
Zhao et al. (Zhao, 2016)	S21	40.00	40.10	2.01	1.80	150.00	0.005	154	183	0.84
	S22	50.10	50.20	1.90	2.50	200.10	0.009	176	205	0.86
Afshan (Afshan, 2014)	S23	80.10	80.10	2.83	3.67	242.00	0.087	362	392	0.92
	S24	59.90	40.00	2.81	3.19	122.10	0.081	235	278	0.84
	S25	119.90	80.00	2.84	3.70	362.00	0.061	431	449	0.96
	S26	60.50	60.50	2.98	2.90	182.20	0.061	338	376	0.90
									Average	0.94
									C.o.V.	0.08
									Average excluding S1 + S18 + S21 + S24	0.97
									C.o.V.	0.06

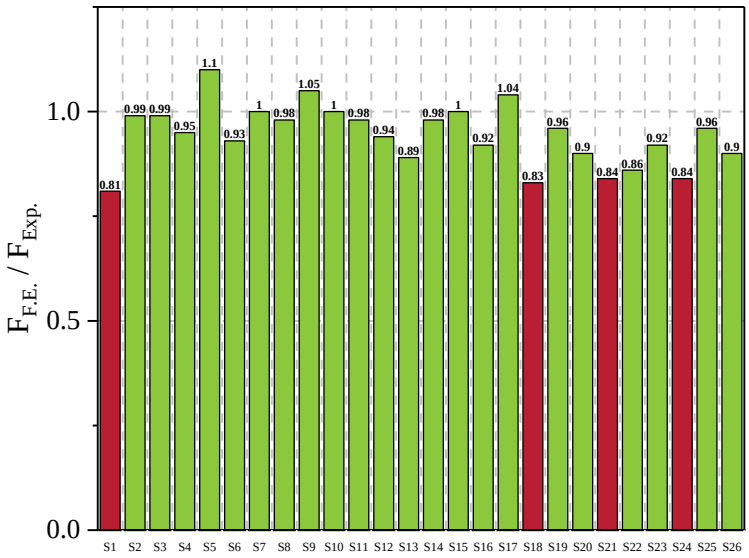

Figure 10. Comparisons between F.E. results and experimental results.

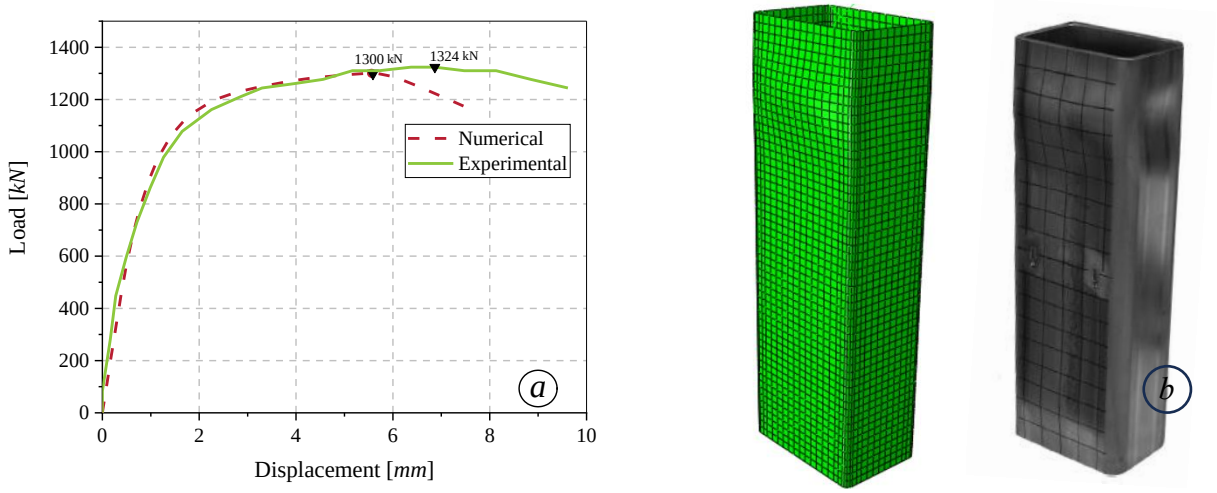

Figure 11. Results for specimen S8 – a) Load-displacement curves – b) Comparison of numerical vs experimental failure modes (Zhao et al. (Zhao, 2015)).

2.7 Parametric studies

Approximately 2 160 simulations were conducted to generate reference results for RHS/SHS cross-sections under simple loading. Key variables included:

- Geometry: 63 sections (42 RHS, 21 SHS), from 150×50 *mm* to 450×450 *mm*;
- Thickness: 2.0-20.45 *mm*, covering slenderness ratios 7.33-71.43 (Table 4);
- Materials: 3 types of stainless steel alloys – 1.4301 (austenitic), 1.4003 (ferritic), and 1.4362 (duplex) – with respective 0.2% proof stresses of 210 N/mm^2, 250 N/mm^2 and 400 N/mm^2, were taken into consideration (Fig. 12);
- Loading: simple load cases, i.e., isolated N, M_y or M_z;
- Analyses: G.M.N.I.A. for ultimate resistance, L.B.A. for local critical buckling and M.N.A. for plastic resistance, yielding $R_{b,L}$, $R_{cr,L}$, and R_{pl} for the O.I.C. framework (Section 3).

Table 4: Cross-sections adopted for the parametric analysis.

Cross-section	Height h [mm]	Width b [mm]	Thickness t [mm]	h / t [–]	b / t [–]
RHS	150	50	6.82	21.99	7.33
RHS	150	75	6.82	21.99	11.00
SHS	150	150	6.82	21.99	21.99
RHS	300	100	13.64	21.99	7.33
RHS	300	150	13.64	21.99	11.00
SHS	300	300	13.64	21.99	21.99
RHS	450	150	20.45	22.00	7.33
RHS	450	225	20.45	22.00	11.00
SHS	450	450	20.45	22.00	22.00
RHS	150	50	3.75	40.00	13.33
RHS	150	75	3.75	40.00	20.00
SHS	150	150	3.75	40.00	40.00
RHS	300	100	7.50	40.00	13.33
RHS	300	150	7.50	40.00	20.00
SHS	300	300	7.50	40.00	40.00
RHS	450	150	11.25	40.00	13.33
RHS	450	225	11.25	40.00	20.00
SHS	450	450	11.25	40.00	40.00
RHS	150	50	2.46	60.98	20.33
RHS	150	75	2.46	60.98	30.49
SHS	150	150	2.46	60.98	60.98
RHS	300	100	4.92	60.98	20.33
RHS	300	150	4.92	60.98	30.49
SHS	300	300	4.92	60.98	60.98
RHS	450	150	7.38	60.98	20.33
RHS	450	225	7.38	60.98	30.49
SHS	450	450	7.38	60.98	60.98
RHS	150	50	2.10	71.43	23.81
RHS	150	75	2.10	71.43	35.71
SHS	150	150	2.10	71.43	71.43
RHS	300	100	4.20	71.43	23.81
RHS	300	150	4.20	71.43	35.71
SHS	300	300	4.20	71.43	71.43
RHS	450	150	6.30	71.43	23.81
RHS	450	225	6.30	71.43	35.71
SHS	450	450	6.30	71.43	71.43
RHS	115	50	2.00	57.50	25.00
RHS	115	75	2.00	57.50	37.50
SHS	115	115	2.00	57.50	57.50
RHS	275	100	4.80	57.29	20.83
RHS	275	150	4.80	57.29	31.25
SHS	275	275	4.80	57.29	57.29
RHS	350	150	6.10	57.38	24.59
RHS	350	225	6.10	57.38	36.89
SHS	350	350	6.10	57.38	57.38
RHS	150	50	3.40	44.12	14.71
RHS	150	75	3.40	44.12	22.06
SHS	150	150	3.40	44.12	44.12
RHS	300	100	6.80	44.12	14.71
RHS	300	150	6.80	44.12	22.06
SHS	300	300	6.80	44.12	44.12
RHS	450	150	10.20	44.12	14.71
RHS	450	225	10.20	44.12	22.06
SHS	450	450	10.20	44.12	44.12
RHS	150	50	5.00	30.00	10.00
RHS	150	75	5.00	30.00	15.00
SHS	150	150	5.00	30.00	30.00
RHS	300	100	11.00	27.27	9.09
RHS	300	150	11.00	27.27	13.64
SHS	300	300	11.00	27.27	27.27
RHS	450	150	18.00	25.00	8.33
RHS	450	225	18.00	25.00	12.50
SHS	450	450	18.00	25.00	25.00

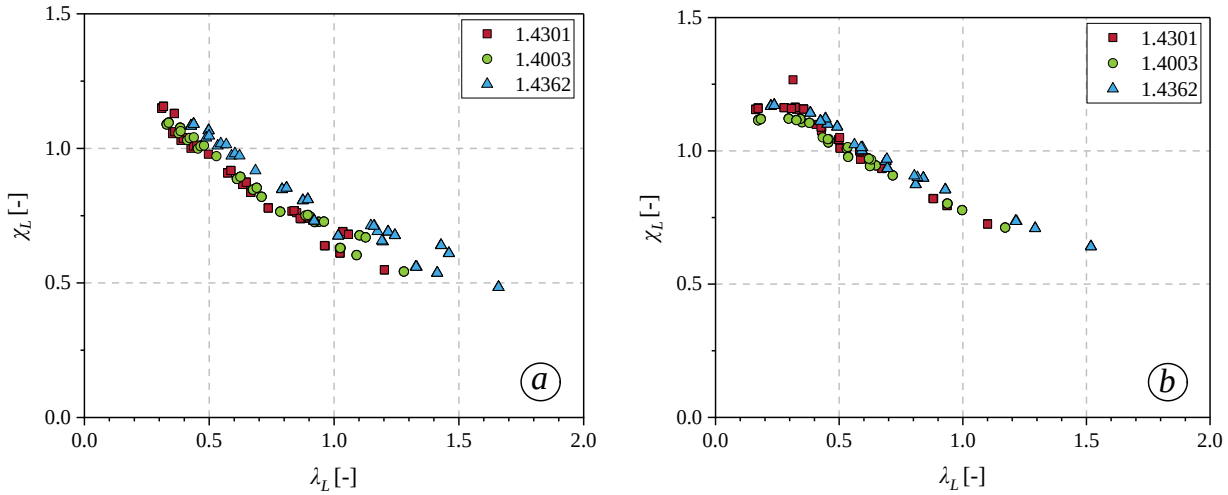

Figure 12. Influence of stainless steel grades on the resistance of – a) Sections in compression – b) Sections under major-axis bending.

3. Proposed O.I.C. design approach

3.1 Fundamentals of the O.I.C.

The Overall Interaction Concept (O.I.C.) is a slenderness-based design method providing direct predictions of cross-section and member resistance. It offers a simple yet accurate framework for capturing resistance-stability interaction, explicitly accounting for imperfection effects and addressing yielding in relation to local and/or global buckling Boissonnade et al. (Boissonnade, 2013) (Boissonnade, 2017) Boissonnade (Boissonnade, 2015). Unlike classification-based approaches, the O.I.C. avoids discontinuities by incorporating geometric imperfections and material non-linearity directly into a unified formulation. The method captures the interaction between yielding and local buckling through a continuous reduction factor, applicable across a wide range of geometries and material grades.

The design procedure is illustrated in Fig. 13. For a given loading case, the plastic resistance ratio R_{pl} is obtained from materially non-linear analysis (M.N.A.), while the elastic local critical resistance ratio $R_{cr,L}$ is determined from linear buckling analysis (L.B.A.). The relative local slenderness is then defined as in Eq. (9).

$$\bar{\lambda}_L = \sqrt{\frac{R_{pl}}{R_{cr,L}}} \tag{9}$$

λ_L directly relates to the reduction factor χ_L, which represents the ratio between ultimate resistance and plastic resistance. The reduction factor χ_L follows an Ayrton–Perry-type expression, calibrated to account for imperfections and post-buckling reserves (Eq. (10)).

$$\chi_L = \frac{1}{\phi_L + \sqrt{\phi_L^{\,2} - \bar{\lambda}_L^{\,\delta}}} \quad with \quad \phi_L = 0.5 \cdot \left[1 + \alpha_L \cdot \left(\bar{\lambda}_L - \lambda_0\right) + \bar{\lambda}_L^{\,\delta}\right] \tag{10}$$

where λ_0 defines the limit between compact and slender behavior and δ stands as a coefficient to account for plate post-buckling effects, particularly in slender sections, while α_L (local geometric

imperfection factor) quantifies the influence of imperfections on resistance. This formulation ensures a smooth transition between plastic-dominated and buckling-dominated regimes.

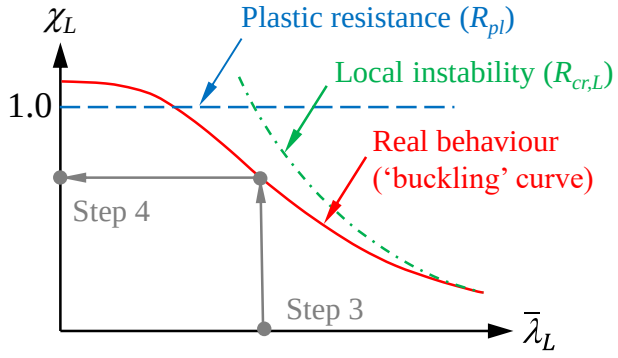

Step 1: R_{pl} Load ratio to reach the plastic 'resistance' limit

Step 2: $R_{cr,L}$ Load ratio to reach the critical 'instability' limit

Step 3: $\bar{\lambda}_L = \sqrt{R_{pl} \,/\, R_{cr,L}}$

Step 4: $\chi_L = f^{\circ}(\bar{\lambda}_L)$

Step 5: $R_{b,L} = \chi_L \,.\, R_{pl}$

Figure 13. Application steps of the O.I.C.

3.2 Determination of additional design parameters

Since the O.I.C. relies on buckling curves expressed as $\chi_L = f^{\circ}(\lambda_L)$ (Fig. 13), an accurate characterization of such buckling curves is essential for accuracy. Yet, as shown in Figs. 12a and 12b, the collected numerical results show a certain degree of dispersion. Consequently, a single safe buckling curve is insufficient. Instead, a series of curves is recommended. Further investigation revealed that it is governed primarily by geometric effects, with limited influence from material properties. To capture geometric effects, the parameter γ_E is introduced, allowing α_L and the post-buckling parameter δ to vary continuously with cross-section proportions.

$$\gamma_E = \frac{h}{t} \cdot \frac{b}{t} \cdot 10^{-3} \tag{11}$$

3.3 Design O.I.C. proposals for stainless steel hollow sections

For compact sections ($\lambda_L \leq \lambda_0$), the reduction factor χ_L is governed by material behavior. The plastic resistance is enhanced using a strain-based formulation, thereby exploiting the pronounced strain hardening of stainless steel. For slender sections ($\lambda_L > \lambda_0$), resistance is controlled by local buckling. The post-buckling response is described through a classical asymptotic formulation, with the influence of imperfections embedded in the calibrated parameters α_L and δ. The final design resistance is obtained as $R_{b,L} = \chi_L.R_{pl}$ ensuring consistency across material grades, loading cases, and geometric slenderness.

Using the extensive parametric database, the O.I.C. parameters λ_0, α_L and δ were calibrated separately for axial compression and uniaxial bending about both principal axes. The resulting values, summarized in Table 5, provide accurate predictions across all investigated sections and loading modes, while maintaining a unified and transparent design format.

Table 5: Design proposals for stainless steel cross-sections under simple load cases.

		Load cases		
		Compression *N*	**Major-axis bending M_y**	**Minor-axis bending M_z**
Welded stainless steel hollow **compact** sections	1.4301	$\bar{\lambda}_{L,N} \leq \lambda_0 = 0.45$ $\chi_{L,N} = -1.04\ \bar{\lambda}_{L,N} + 1.468$	$\bar{\lambda}_{L,My} \leq \lambda_0 = 0.55$ $\chi_{L,My} = -0.61\ \bar{\lambda}_{L,My} + 1.3355$	$\bar{\lambda}_{L,Mz} \leq \lambda_0 = 0.55$ $\chi_{L,Mz} = -0.52\ \bar{\lambda}_{L,Mz} + 1.286$
	1.4003	$\bar{\lambda}_{L,N} \leq \lambda_0 = 0.45$ $\chi_{L,N} = -0.92\ \bar{\lambda}_{L,N} + 1.414$	$\bar{\lambda}_{L,My} \leq \lambda_0 = 0.55$ $\chi_{L,My} = -0.43\ \bar{\lambda}_{L,My} + 1.2365$	$\bar{\lambda}_{L,Mz} \leq \lambda_0 = 0.55$ $\chi_{L,Mz} = -0.42\ \bar{\lambda}_{L,Mz} + 1.231$
	1.4362	$\bar{\lambda}_{L,N} \leq \lambda_0 = 0.55$ $\chi_{L,N} = -0.84\ \bar{\lambda}_{L,N} + 1.462$	$\bar{\lambda}_{L,My} \leq \lambda_0 = 0.6$ $\chi_{L,My} = -0.6\ \bar{\lambda}_{L,My} + 1.36$	$\bar{\lambda}_{L,Mz} \leq \lambda_0 = 0.6$ $\chi_{L,Mz} = -0.5\ \bar{\lambda}_{L,Mz} + 1.3$
Welded stainless steel hollow **slender** sections	1.4301	$\bar{\lambda}_{L,N} > \lambda_0 = 0.45$ $\alpha_L = 0.0715.\gamma_E + 0.104$ $\delta = -0.0285.\gamma_E + 0.269$	$\bar{\lambda}_{L,My} > \lambda_0 = 0.55$ $\alpha_L = 0.0241.\gamma_E + 0.0555$ $\delta = -0.0597.\gamma_E + 0.4315$	$\bar{\lambda}_{L,Mz} > \lambda_0 = 0.55$ $\alpha_L = -0.016.\gamma_E + 0.182$ $\delta = 0.281.\gamma_E - 0.109$
	1.4003			
	1.4362	$\bar{\lambda}_{L,N} > \lambda_0 = 0.55$ $\alpha_L = 0.1245.\gamma_E + 0.04$ $\delta = -0.242.\gamma_E + 0.359$	$\bar{\lambda}_{L,My} > \lambda_0 = 0.6$ $\alpha_L = 0.0385.\gamma_E + 0.0088$ $\delta = -0.0635.\gamma_E + 0.406$	$\bar{\lambda}_{L,Mz} > \lambda_0 = 0.6$ $\alpha_L = -0.02.\gamma_E + 0.129$ $\delta = 0.147.\gamma_E + 0.211$

4. Accuracy of O.I.C.-based proposals

This section evaluates and compares the resistance predictions of the proposed O.I.C. design approach with results from the reference finite-element (F.E.) database and with resistances estimated using established design standards, including Eurocode 3 (EC3), and A.I.S.C.

The response of compact sections is mainly governed by the mechanical properties of the stainless steel alloy, whereas slender sections are primarily controlled by the geometric parameter γ_E. An increase in the 0.2% proof stress $\sigma_{0.2}$ leads to higher reduction factor χ_L and, consequently, enhanced ultimate resistance, as illustrated in Fig. 12. This behavior is largely attributed to the pronounced strain-hardening characteristics of stainless steel (see Fig. 1). In contrast, the behavior of slender sections remains dominated by geometric effects.

The outcomes of the O.I.C. design approach for the simple load cases – axial compression (N), major-axis bending (M_y), and minor-axis bending (M_z) – are presented in Figs. 14a to 16b. Resistance predictions from finite-element (F.E.) simulations, Eurocode 3 (EC3) and the American Institute of Steel Construction (A.I.S.C.) are included for comparison. In Figs. 14a, 15a, and 16a, the results are expressed as $\chi_L = f°(\lambda_L)$, while the corresponding statistical assessments are shown in Figs. 14b, 15b, and 16b. The histograms illustrate the ratio $\chi_{L,\,Ref.} / \chi_{L,\,F.E.}$, where $\chi_{L,\,Ref.}$ represents the resistance predicted by the design standard and $\chi_{L,\,F.E.}$ that obtained from F.E. analyses. Ratios below unity indicate conservative predictions, whereas values above unity denote unconservative estimates. These comparisons enable a clear assessment of the accuracy and consistency of each design approach under different loading conditions. The most reliable predictions are those that remain slightly conservative, with ratios close to 1.0, while narrow histogram distributions indicate robust and consistent performance, in contrast to wider spreads that reflect increased scatter and reduced accuracy.

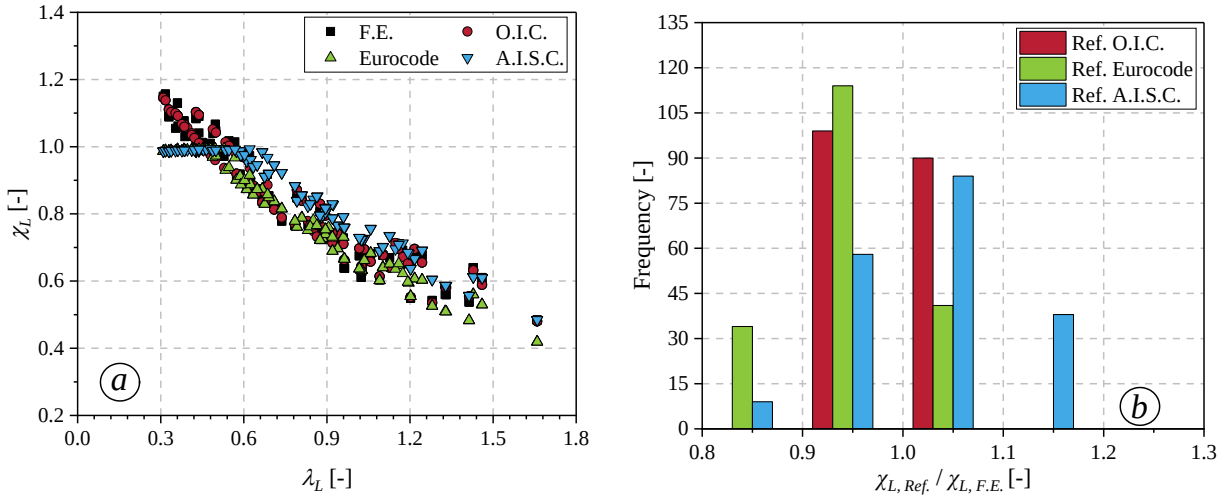

Figure 14. Performance of stainless steel welded sections in compression N – a) $\chi_L - \lambda_L$ O.I.C. plot – b) Statistical distribution.

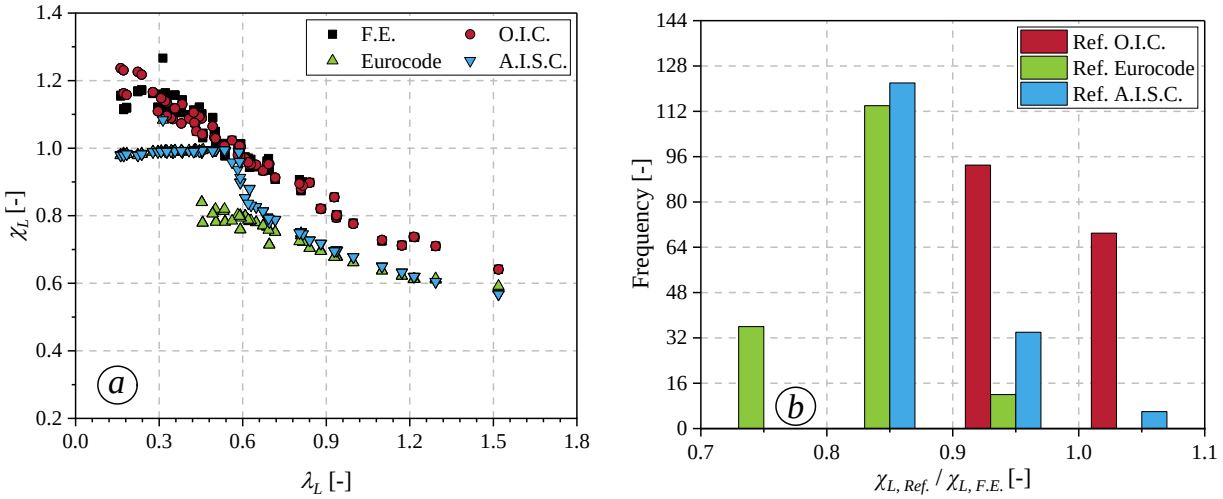

Figure 15. Performance of stainless steel welded sections in compression M_y – a) $\chi_L - \lambda_L$ O.I.C. plot – b) Statistical distribution.

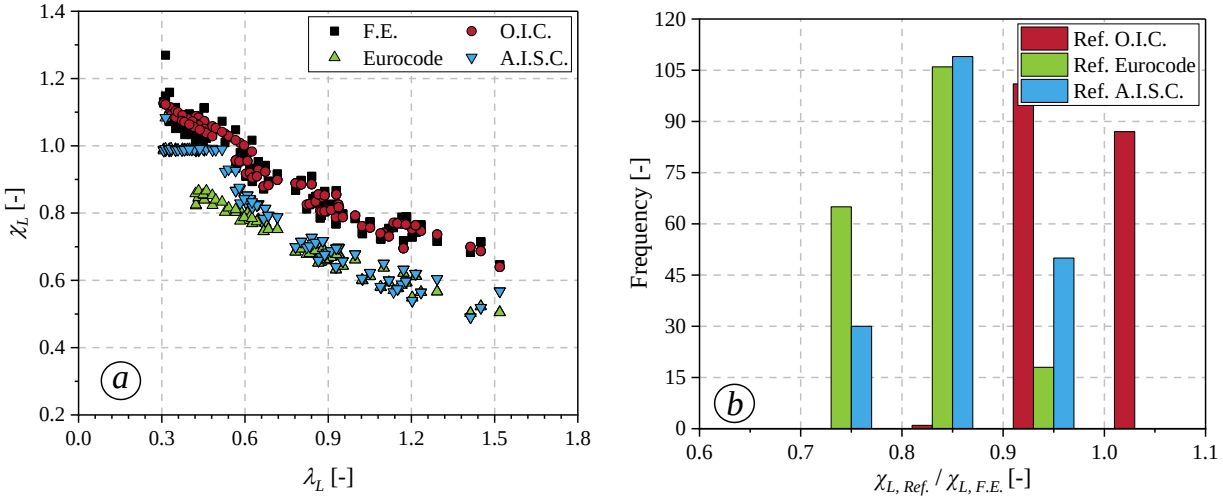

Figure 16. Performance of stainless steel welded sections in compression M_z – a) $\chi_L - \lambda_L$ O.I.C. plot – b) Statistical distribution.

The histogram comparisons reveal several key findings. The proposed O.I.C. method accurately captures the behavior of both compact and slender stainless steel hollow sections, demonstrating excellent agreement with the reference finite-element results across all simple load cases. The reliability of the proposed interaction curves is further illustrated in Figs. 14a, 15a, and 16a. The high accuracy achieved for compact sections is primarily attributed to the explicit consideration of strain-hardening effects in the O.I.C. approach, which are neglected in conventional design standards. By contrast, alternative design provisions either lead to unsafe resistance estimates, as observed in the A.I.S.C. specifications, or produce overly conservative predictions, as in Eurocode 3.

Eurocode 3 adopts an overly conservative approach, mainly due to its cross-section classification method, the assumption of pin-ended plate support, and the neglect of flange-web interaction. For Class 3 sections, resistance is limited to the elastic capacity, resulting in discontinuities in the interaction curves, particularly under major and minor axes bending. The omission of partial yielding effects leads to an overly conservative estimation of cross-sectional resistance. Similarly,

the A.I.S.C. provisions disregard strain-hardening at low slenderness, leading to unsafe predictions in compression and major-axis bending and excessive conservatism in minor-axis bending. Overall, the results highlight a clear lack of consistency in current standards, which combine excessive conservatism with the potential for unsafe predictions.

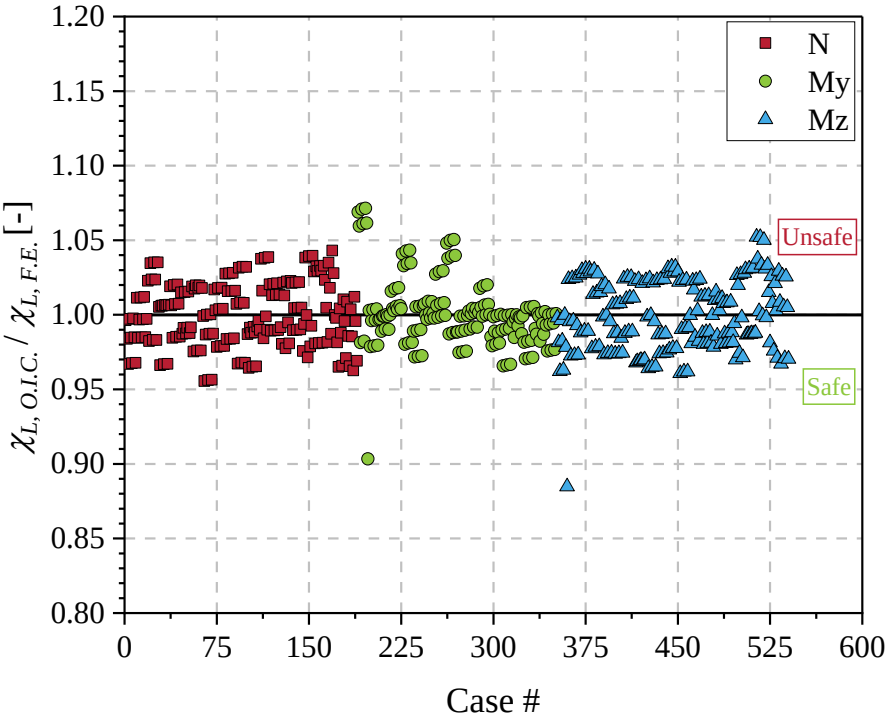

Figure 17. Proposal performance across simple load cases.

The accuracy and reliability of the proposed O.I.C. method are assessed against finite-element results for simple load cases – compression, major-axis bending, and minor-axis bending – as shown in Fig. 17, which provides an overall evaluation of the approach. Ratios of $\chi_{L,\,O.I.C.} / \chi_{L,\,F.E}$ below unity indicate conservative predictions, while values above unity denote unsafe estimates. Most results fall within an acceptable range, concentrated closely near unity. A limited number of cases slightly exceed 1.00 but remain below 1.10; the marginal deviations are acceptable when considering typical safety factors, with only a few overly conservative predictions observed. Overall, the results confirm the accuracy, consistency, and reliability of the O.I.C. method.

A quantitative assessment is presented in Table 6, which summarizes the statistical performance of the O.I.C. approach for simple load cases. With an average ratio of 1.00 and a maximum standard deviation of only 2.25%, the method demonstrates a high level of accuracy and consistency. The most conservative value, corresponding to minor-axis bending (0.88), is considered reasonable, while no critical unsafe outcomes are identified, with a maximum ratio of 1.07 for major-axis bending and no values exceeding 1.10. The few marginally unsafe cases can be further reduced through the application of the safety factors outlined in Section 5.

A comparison with existing standards further highlights the advantages of the O.I.C. method. As shown in Table 6, Eurocode 3 exhibits a conservative average ratio of 0.87 with a coefficient of variation (C.o.V.) of 8.92%, while the A.I.S.C. provisions show a higher scatter (C.o.V. = 11.23%) and a critical unsafe value of 1.19. In contrast, the O.I.C. method provides more accurate and

consistent resistance predictions, offering clear reliability benefits for practical design while remaining simple and straightforward to apply.

Table 6: Statistical evaluation of $\chi_{L,\,Ref.}$ / $\chi_{L,\,F.E.}$ ratio for welded stainless steel sections based on simple load cases.

Load cases	Number of cases	Proposals	Mean	C.o.V.	Max.	Min.	< 0.88 [%]	< 0.98 [%]	> 1.05 [%]	> 1.10 [%]
Compression N	189	O.I.C.	1.00	2.11%	1.04	0.96	0.00%	16.40%	0.00%	0.00%
		EC3	0.95	5.49%	1.05	0.85	11.11%	58.20%	0.00%	0.00%
		A.I.S.C.	1.04	8.33%	1.19	0.85	4.76%	25.40%	49.74%	20.11%
Major-axis bending M_y	162	O.I.C.	1.00	2.26%	1.07	0.90	0.00%	12.35%	4.32%	0.00%
		EC3	0.84	5.60%	0.95	0.74	79.63%	100.00%	0.00%	0.00%
		A.I.S.C.	0.89	5.38%	1.02	0.81	53.09%	91.98%	0.00%	0.00%
Minor-axis bending M_z	189	O.I.C.	1.00	2.39%	1.05	0.88	0.00%	22.75%	1.59%	0.00%
		EC3	0.82	6.11%	0.96	0.73	88.89%	100.00%	0.00%	0.00%
		A.I.S.C.	0.86	6.95%	0.98	0.72	61.90%	99.47%	0.00%	0.00%
All load cases	540	O.I.C.	1.00	2.25%	1.07	0.88	0.00%	17.41%	1.85%	0.00%
		EC3	0.87	8.92%	1.05	0.73	58.89%	85.37%	0.00%	0.00%
		A.I.S.C.	0.93	11.23%	1.19	0.72	39.26%	71.30%	17.41%	7.04%

5. Reliability analyses

A reliability analysis was conducted in accordance with Annex D of EN 1990 (EN 1990,2002), which is associated with higher safety margins than those prescribed by the A.I.S.C. The analysis was performed to further evaluate the accuracy of the proposed O.I.C.-based design equations for hollow stainless steel sections under simple load cases. Each design standards employs a safety factor, denoted as ϕ in A.I.S.C. and γ_{M0} in the Eurocode framework ($\gamma_{M0} \approx 1 / \phi$).

Owing to the absence of experimental data for welded stainless steel hollow sections, the evaluation relied exclusively on the finite element results generated in Section 2. Table 7 provides a summary of the main parameters adopted in the statistical evaluation of all datasets, where n denotes the number of numerical reference results considered, $K_{d,n}$ is the design fractile factor, b represents the mean correction factor obtained by the least-squares method, V_δ is the coefficient of variation of the error terms, V_r is the combined C.o.V. accounting for uncertainties derived from both the design model and the basic variables, calculated based on a simplified approach (Afshan et al. (Afshan, 2015)) using Eqs. (12) and (13), and γ_{M0} are the required partial resistance safety factors. To account for uncertainties in material properties, section dimensions, and the accuracy of the design model, an additional safety margin of approximately 10% is recommended when evaluating cross-section resistance, as the predicted γ_{M0} values remain below 1.10.

According to Afshan et al. (Afshan, 2015)), the representative over-strength factors and corresponding coefficients of variation for material yield strength (V_{mat}) are 1.3 and 0.06 for austenitic, 1.2 and 0.045 for ferritic, and 1.1 and 0.03 for duplex stainless steels, respectively. A coefficient of variation of 0.05 is adopted to account for geometric variability (V_{geom}).

$$V_r^{\,2} = V_\delta^{\,2} + V_{rt}^{\,2} \tag{12}$$

$$V_{rt}^{\,2} = V_{mat}^{\,2} + V_{geom}^{\,2} \tag{13}$$

Table 7: Reliability analysis results for the design of hollow stainless steel sections subjected to simple load cases (excluding tail approximation).

Proposals	***n***	$k_{d,n}$	***b***	V_δ	V_r	γ_{M0}
O.I.C.	540	3.108	1.000	0.023	0.071	1.04
EC3		3.108	1.142	0.089	0.111	1.03
A.I.S.C.		3.108	1.080	0.110	0.129	1.15

Table 8: Reliability analysis results for the design of hollow stainless steel sections subjected to simple load cases (including tail approximation).

Proposals	***n***	$k_{d,n}$	***b***	V_δ	V_r	γ_{M0}
O.I.C.	532	3.109	0.999	0.021	0.071	1.04
EC3	356	3.118	1.100	0.064	0.094	1.00
A.I.S.C.	464	3.111	1.065	0.097	0.118	1.12

Table 7 shows that the A.I.S.C. design model yields a large number of overly conservative predictions, resulting in γ_{M0} values significantly higher than those obtained using the O.I.C. and Eurocode 3 approaches. The variation of γ_{M0} was further investigated using the tail approximation (T.A.) technique (Taras et al. (Taras, 2017)), in which only the distribution tail is retained to obtain more representative datasets for each design model. Fig. 18a presents the E.C.3. results, where 356 out of 540 data points were retained in the tail. In this figure, resistance values (r_e) derived from finite-element (F.E.) simulations are compared with the corresponding E.C.3. predictions (r_t). For normalized distributional comparison, the data are standardized along the vertical axis by converting cumulative probabilities into equivalent standard deviation values. Under an ideal log-normal resistance model, all points would align along the corresponding regression lines.

Fig. 18b illustrates the relationship between the number of data points retained in the tail approximation and the evolution of γ_{M0}. The comparison includes the O.I.C. method and other design approaches, using the previously defined parameters, V_r, V_{mat}, and V_{geom}. The corresponding minimum safety factors are summarized in Table 8. As expected, all tail approximations lead to relatively low γ_{M0} values. The results show that Eurocode 3 yields γ_{M0} = 1.00, confirming the adequacy of the value recommended in EN 1993-1-4. The O.I.C. approach may also be applied safely and reliably to stainless steel hollow sections under simple load cases, with a corresponding γ_{M0} of 1.04 (for 532 retained data points), which is fully acceptable despite being slightly higher than that of Eurocode 3. By contrast, the A.I.S.C. provisions result in the highest γ_{M0} value, equal to 1.12.

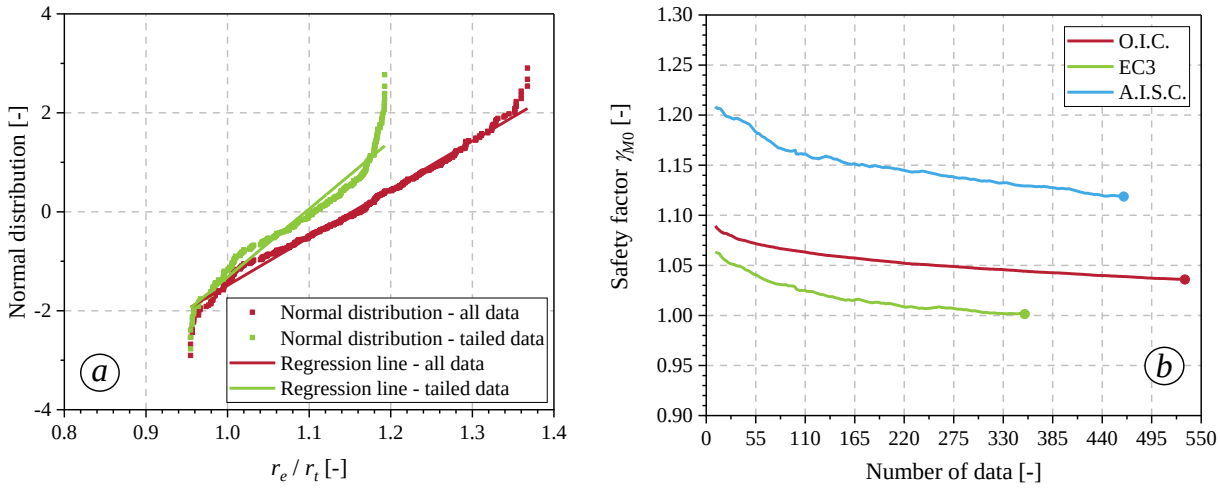

Figure 18. a) Tail approximation for EC3 with 356 data points – b) Evolution of safety factors γ_{M0} with number of data points retained in the tail approximations.

6. Conclusions and future works

This study investigated the local buckling behavior of welded stainless steel rectangular and square hollow sections (RHS/SHS) under simple load cases. A database of 26 experimental tests was compiled to validate advanced non-linear shell finite-element models. An extensive parametric study was then conducted, covering 63 cross-sections, three stainless steel grades (1.4301, 1.4003, and 1.4362), three load cases (N, M_y, and M_z), and three analysis types (G.M.N.I.A., L.B.A., and M.N.A.). The results formed the basis of evaluating new design equations developed using the Overall Interaction Concept (O.I.C.) for welded stainless steel hollow sections. The accuracy of the proposed O.I.C. approach and two existing design standards was assessed against the numerical results, demonstrating that the O.I.C. method significantly improves resistance predictions and provides a robust and practical design alternative. A reliability analysis in accordance with EN 1990 further confirms the consistency and reliability of the proposed framework.

While previous studies have established the O.I.C. framework for various welded I-section configurations, its extension to more complex cross-sectional geometries remain unexplored. Future research should therefore focus on extending the approach to complex section forms and on addressing additional instability phenomena, starting with global buckling and progressing toward the interaction between local and global instability modes.

References

Afshan, S. (2014). Structural behaviour of cold-formed stainless steel tubular members (PhD thesis). Imperial College London.

Afshan, S., Francis, P., Baddoo, N. R., & Gardner, L. (2015). Reliability analysis of structural stainless steel design provisions. Journal of Constructional Steel Research, 114, 293–304.

Abaqus G. (2011). Abaqus 6.11. Providence, RI, USA: Dassault Systemes Simulia Corporation.

Abaqus Analysis User's Guide, Vol. 4, p. 1128.

American Institute of Steel Construction (AISC). (2013). Specification for Structural Steel Buildings (ANSI/AISC 360–10). Chicago, IL: AISC.

Ashraf, M., Gardner, L., & Nethercot, D. A. (2005). Strength of the corner regions of stainless steel cross sections. Journal of Constructional Steel Research, 61(1), 37–52.

Ashraf, M., Gardner, L., & Nethercot, D. (2006). Compression strength of stainless steel cross-sections. Journal of Constructional Steel Research, 62(1–2), 105–115.

Ayrton, W. E., & Perry, J. (1886). On struts. The Engineer, 62.

Boissonnade, N. (2015). Application of the overall interaction concept to the design of steel sections and members. Proceedings of the 9th European Solid Mechanics Conference (ESMC 2015), Madrid, Spain.

Boissonnade, N., Hayek, M., Saloumi, E., & Nseir, J. (2017, August). An Overall Interaction Concept for an alternative approach to steel members design. Journal of Constructional Steel Research, 135, 199–212.

Boissonnade, N., Nseir, J., & Saloumi, E. (2013). The overall interaction concept: An alternative approach to the stability and resistance of steel sections and members. Proceedings of the 2013 SSRC Annual Stability Conference, Saint Louis, USA.

BSK 99. (2003). Swedish regulations for steel structures. Boverket, Karlskrona, Sweden.

CEN. (2015). EN 1993-1-4:2006+A1:2015 – Eurocode 3: Design of steel structures – Part 1-4: General rules – Supplementary rules for stainless steels (including amendment A1). Brussels: European Committee for Standardization (CEN).

Cruise, R. B., & Gardner, L. (2008). Strength enhancements induced during cold forming of stainless steel sections. Journal of Constructional Steel Research, 64(11), 1310–1316.

Dahboul, S., Verma, P., Li, L., Dey, P., & Boissonnade, N. (2025). O.I.C.-based design of extruded aluminium rectangular hollow sections under simple load cases. Structures, 79, 105–118.

ECCS. (1976). Manual on stability of steel structures – Part 2.2: Mechanical properties and residual stresses (2nd ed.). Brussels: ECCS Publication.

ECCS. (1984). Ultimate limit state calculation of sway frames with rigid joints. Technical Committee 8 – Structural Stability, Technical Working Group 8.2 – System. Publication No. 33. Brussels: ECCS.

Ellobody, E., & Young, B. (2005). Structural performance of cold-formed high strength stainless steel columns. Journal of Constructional Steel Research, 61(12), 1631–1649.

European Committee for Standardization. (2002). EN 1990: Eurocode – Basis of Structural Design. Brussels, Belgium: CEN.

European Convention for Constructional Steelwork (ECCS). (1976). Manual on stability of steel structures – Part 2.2: Mechanical properties and residual stresses (2nd ed.). Brussels: ECCS Publication.

European Convention for Constructional Steelwork (ECCS). (1984). Ultimate limit state calculation of sway frames with rigid joints. Technical Committee 8 – Structural Stability, Technical Working Group 8.2 – System. Publication No. 33. Brussels: ECCS.

Gagné, A.-S., Gérard, L., & Boissonnade, N. (2020). Design of stainless steel cross-sections for simple load cases with the Overall Interaction Concept (O.I.C.). Journal of Constructional Steel Research, 168, Article 105936.

Gardner, L. (2008). Aesthetics, economics and design of stainless steel structures. Advanced Steel Construction, 4(2), 113–122.

Gardner, L. (2019). Stability and design of stainless steel structures – Review and outlook. Thin-Walled Structures, 141, 208–216.

Gardner, L., & Ashraf, M. (2006). Structural design for non-linear metallic materials. Engineering Structures, 28(6), 926–934.

Gardner, L., & Nethercot, D. (2004). Numerical modeling of stainless steel structural components – a consistent approach. Journal of Structural Engineering, 130(10), 1586–1601.

Gardner, L., & Nethercot, D. A. (2004). Experiments on stainless steel hollow sections – Part 1: Material and cross-sectional behaviour. Journal of Constructional Steel Research, 60(9), 1291–1318.

Gardner, L., & Ng, K. T. (2006). Temperature development in structural stainless steel sections exposed to fire. Fire Safety Journal, 41(3), 185–203.

Gardner, L., Yun, X., & Walport, F. (2023). The Continuous Strength Method – Review and outlook. Engineering Structures, 275(Part A), Article 114924.

Hayeck, M. (2016). Development of a new design method for steel hollow section members resistance (Doctoral dissertation, Université de Liège, Belgium; in collaboration with University of Applied Sciences of Western Switzerland; Fribourg, and Saint Joseph University; Beirut).

Hill, H. N. (1944). Determination of stress–strain relations from offset yield strength values. Technical note No. 927, Washington DC: National advisory committee for aeronautics.

Huang, Y., & Young, B. (2012). Material properties of cold-formed lean duplex stainless steel sections. Thin-Walled Structures, 54, 72–81.

Karren, K. W. (1967). Corner properties of cold-formed steel shapes. Journal of the Structural Division, ASCE, 93(ST1), 401–432.

Maquoi, R., & Rondal, J. (1978). Mise en équation des nouvelles courbes européennes de flambement. Construction Métallique, no. 1, 17–29.

Mirambell, E., & Real, E. (2000). On the calculation of deflections in structural stainless steel beams: an experimental and numerical investigation. Journal of Constructional Steel Research, 54(1), 109–133.

Nseir, J. (2015). Development of a new design method for the cross-section capacity of steel hollow sections (Doctoral dissertation, Université de Liège, Belgium; Saint Joseph University; Beirut).

Nseir, J., Hayeck, M., Saloumi, E., & Boissonnade, N. (2016). Influence of imperfections on the local buckling response of hollow structural shapes. Proceedings of the 2016 SSRC Annual Stability Conference, Orlando, USA.

Nseir, J., Saloumi, E., Hayeck, M., & Boissonnade, N. (2015). A new design method for hollow steel sections: the Overall Interaction Concept. Proceedings of the 15th International Symposium on Tubular Structures (ISTS15), Rio de Janeiro, Brasil.

Paquet, J. (2021). Development of a new design method for the cross section capacity of steel open sections at high temperatures (M.S. thesis). Université Laval, Québec, Canada.

Quach, W. M., Teng, J. G., & Chung, K. F. (2009). Residual stresses in press-braked stainless steel sections, Part I: Coiling and uncoiling of sheets. Journal of Constructional Steel Research, 65(9), 1803–1815.

Quach, W. M., Teng, J. G., & Chung, K. F. (2009). Residual stresses in press-braked stainless steel sections, Part II: Press-braking operations. Journal of Constructional Steel Research, 65(9), 1816–1826.

Ramberg, W., & Osgood, W. R. (1943). Description of stress–strain curves by three parameters. Technical note No. 902, Washington DC: National advisory committee for aeronautics.

Rasmussen, K. J. R. (2003). Full-range stress–strain curves for stainless steel alloys. Journal of Constructional Steel Research, 59(1), 47–61.

SCI. (2017). Design manual for structural stainless steel (4th ed.). Ascot, UK: The Steel Construction Institute.

Taras, A., Dehan, V., da Silva, L. S., Marques, L., & Tankova, T. (2017). Guideline for the Safety Assessment of Design Rules for Steel Structures in Line with EN 1990 (Deliverable D1.1, SAFEBRICTILE, Grant Agreement RFSR-CT-2013-00023). European Commission.

Van den Berg, G. J., & van der Merwe, P. (1992). Prediction of corner mechanical properties for stainless steels due to cold forming. In: Proceedings of the 11th International Specialty Conference on Cold-Formed Steel Structures, 571–586.

Withers, P. J., & Bhadeshia, H. K. D. H. (2001). Residual stress. Part 2 – Nature and origins. Materials Science and Technology, 17(4), 366–375.

Yuan, H. X., Wang, Y. Q., Shi, Y. J., & Gardner, L. (2014). Residual stress distributions in welded stainless steel sections. Thin-Walled Structures, 83, 115–126.

Young, B., & Lui, W. M. (2005). Behavior of cold-formed high strength stainless steel sections. Journal of Structural Engineering, 131(11), 1738–1745.

Zhao, O., Rossi, B., Gardner, L., & Young, B. (2015). Behaviour of structural stainless steel cross-sections under combined loading – Part I: Experimental study. Engineering Structures, 89, 236–246.

Zhao, O., Rossi, B., Gardner, L., & Young, B. (2016). Experimental and numerical studies of ferritic stainless steel tubular cross-sections under combined compression and bending. Journal of Structural Engineering, 142(2), 04015110.